RESEARCH PAPER

Electron beam-induced structural transformations of MoO_3 and MoO_{3-x} crystalline nanostructures

D. E. Diaz-Droguett · A. Zuñiga · G. Solorzano · V. M. Fuenzalida

Abstract Electron beam-induced damage and structural changes in MoO_3 and MoO_{3-x} single crystalline nanostructures were revealed by in situ transmission electron microscopy (TEM) examination (at 200 kV) after few minutes of concentrating the electron beam onto small areas (diameters between 25 and 200 nm) of the samples. The damage was evaluated recording TEM images, while the structural changes were revealed acquiring selected area electron diffraction patterns and high resolution transmission electron microscopy (HRTEM) images after different irradiation times. The as-received nanostructures of orthorhombic MoO_3 were transformed to a Magnéli's phase of the oxide (γ-Mo_4O_{11}) after ~10 min of electron beam irradiation. The oxygen loss from the oxide promoted structural changes. HRTEM observations showed that, in the first stage of the reduction, oxygen vacancies generated by the electron beam are accommodated by forming crystallographic shear planes. At a later stage of the reduction process, a polycrystalline structure was developed with highly oxygen-deficient grains. The structural changes can be attributed to the local heating of the irradiated zone combined with radiolysis.

Keywords Electron beam · Molybdenum oxide · Nanostructures · Magnéli's phase · TEM

D. E. Diaz-Droguett (✉) · V. M. Fuenzalida
Departamento de Fisica, Facultad de Ciencias Fisicas y
Matematicas, Universidad de Chile, Santiago, Chile
e-mail: dodiaz@fis.puc.cl

Present Address:
D. E. Diaz-Droguett
Departamento de Fisica, Facultad de Fisica, Pontificia
Universidad Catolica de Chile, Santiago, Chile

A. Zuñiga
Departamento de Ingenieria Mecánica, Facultad de
Ciencias Fisicas y Matematicas, Universidad de Chile,
Santiago, Chile

G. Solorzano
Departamento de Ciencia dos Materiais e Metalurgia,
DCMM, PUC-RIO, Rio de Janeiro, Brazil

Introduction

Molybdenum is known to form MoO_2 and MoO_3 oxides, and well-defined suboxides denoted with the general formula Mo_nO_{3n-1} (e.g., Mo_4O_{11}, Mo_5O_{14}, Mo_8O_{23}, Mo_9O_{26}), known as Magnéli's phases of the molybdenum oxide (Magnéli [1953]; Vincent and Marezio [1989]). MoO_3 has a layered orthorhombic structure with layers parallel to the (010) lattice plane bonded together by van der Waals forces. Each layer consists of two interleaved planes of distorted MoO_6 octahedra held together by covalent forces (Henrich and Cox [1994]). Only oxygen ions are exposed on the surface of these layers resulting in a quite chemically inert surface at room temperature. However, when the MoO_3 (010) surface is exposed to electron or ion

beams, even of relatively low energy, or to near-bandgap ultraviolet photons (Fleisch et al. 1986), the surface becomes reduced. The ease of reduction occurs because of the many molybdenum suboxides (Magnéli's phases) that are stable in the bulk. Most studies reporting on structural changes of MoO_3 under irradiation in an electron microscope concluded that the MoO_2 oxide was the product of reduction (Bursill 1969; Bertrand and Dufour 1980). Surface oxygen defects are induced by the incidence of the electron beam. These oxygen vacancies are proposed to be consumed in the formation of crystallographic shear (CS) planes forming oxygen-deficient superlattices. At higher electron beam currents, tiny MoO_2 crystals were detected as the product of MoO_3 reduction (Bursill 1969), where topotactic mechanisms of phase transformation from MoO_3 to MoO_2 have been suggested by Bertrand and Dufour (1980) and Delannay (1982). In recent years, Su (2002) reported an unknown phase of molybdenum oxide with cation valence lower than $+4$. Wang et al. (2004) reported the transformation of MoO_3 to MoO_2 induced by an electron beam at low current density (~ 1.3 A/cm^2) while MoO with a rock-salt structure was suggested to be the final phase in the MoO_3 reduction at high current density (~ 57.6 A/cm^2). These reports were based on the study of MoO_3 in the bulk form (commercial powder of MoO_3) as the starting material. However, studies on the reduction and phase transformations of MoO_3 crystalline nanostructures due to the electron beam irradiation have not been reported. Diaz-Droguett et al. (2008a) reported the effects of the electron beam on MoO_3 amorphous nanoporous structures which lead to crystallization of the material in few minutes with no destruction of the porous morphology. The knowledge of electron beam-induced structure changes helps to understand the differences in the reduction behavior, phase stability and phase transition routes of MoO_3 nanostructures as compared to its bulk form. Moreover, the generation of molybdenum suboxides nanostructures by electron irradiation and the knowledge of the resulting structures may be important in catalysis. Molybdenum oxide-based catalysts are used extensively in the selective oxidation of hydrocarbons where the catalytically active phase is neither MoO_3 nor MoO_2 but rather a partially reduced molybdenum oxide (Grasselli 1999; Bettahar et al. 1996; Haber and Lalik 1997).

This study reports on the structural transformations of MoO_3 and MoO_{3-x} crystalline nanostructures induced by electron beam irradiation when examined under a transmission electron microscope (TEM). The study was performed on individual nanostructures recording TEM images, selected area electron diffraction (SAED) patterns and energy dispersive X-ray spectra (EDS) at different irradiation times.

Experimental

Preparation of MoO_3 and MoO_{3-x} nanostructures

The nanostructures were grown in a simple one-step process by evaporating MoO_3 from a tungsten resistive boat in an atmosphere of either helium (AGA, 99.995%, $O_2 < 5$ ppm and $H_2O < 2$ ppm) or hydrogen (AGA, 99.995%, $O_2 < 5$ ppm and $H_2O < 4$ ppm) at a pressure of 600 Pa. The tungsten boat was heated to temperatures between 650 and 950 °C. The samples grown in vapor phase were deposited on a collecting surface cooled with liquid nitrogen and it located 75 mm above the tungsten boat. Each preparation condition is determined by the type of gas and the boat temperature which define the evaporation rate. The preparation condition of each sample will be represented by the nomenclature "condition" (gas, tungsten source temperature), which will be used throughout the article.

The experimental set up and the procedure for the preparation of the nanostructures have been already detailed elsewhere (Diaz-Droguett et al. 2008a, b; Diaz-Droguett and Fuenzalida 2010).

Characterization

The study of the electron beam effects on the molybdenum oxide nanostructures were performed in two transmission electron microscopes (TEM/HRTEM JEOL 2010 and FEI TECNAI F20 G^2 TEM) both operating at 200 kV and under diffraction and phase contrast modes. These TEMs were equipped with EDS and SAED. The electron irradiation on individual nanostructures was performed concentrating the electron beam on circular areas with diameters between 50 and 200 nm depending on the size of the nanostructure examined. The beam intensity was kept constant varying the irradiation times and the electron

doses depending on the areas illuminated by the beam. The operating conditions of the TEM in a typical experiment of irradiation were the following: emission current ~ 67 μA; extraction voltage = 3,800 V; gun lens = 3; aperture C2 = 200 μm.

The effects caused by the electron beam exposition were monitored recording TEM images (multi beam and bright/dark field images) at different irradiation times; the sequential changes of the structure of the samples were studied by SAED patterns and high resolution transmission electron microscopy (HRTEM) images; and the chemical changes of the reduction process were monitored acquiring in situ EDS spectra after different irradiation times.

For the TEM examination, the molybdenum oxide nanostructures were dispersed in isopropyl alcohol using an ultrasonic bath and then trapped on the microscope copper grid.

Results

X-ray photoelectron spectroscopy (XPS): oxidation states of the as-prepared samples

XPS measurements of the as-prepared crystalline nanostructures detected only molybdenum in its 6+ oxidation state in the samples grown under helium at 600 Pa, exhibiting the same chemical composition as that of the source material (MoO_3 pellet). Molybdenum in its 6+ as well as 5+ oxidation states were detected in the crystalline samples grown under hydrogen at the same pressure revealing the presence of a suboxide of the MoO_{3-x} form (Diaz-Droguett and Fuenzalida 2010).

Figure 1 shows Mo 3d levels spectra and their curve fits obtained from samples grown under similar conditions of preparation (pressure and source temperature) varying only the carrier gas. The spectra of Fig. 1a, b correspond to samples grown under the conditions (He, 785 °C) and (H_2, 777 °C), respectively. In Fig. 1a, the best fit assigned 232.5 eV to the $3d_{5/2}$ level and 235.6 eV to the $3d_{3/2}$ level, with a full width at half maximum (FWHM) of 2.3 and 2.2 eV, respectively. These binding energies are very close to the reported values for Mo^{6+}: 232.6 eV and 235.8 for the $3d_{5/2}$ and $3d_{3/2}$ levels (Wagner et al. 1979), respectively. On the other hand, the best fit in Fig. 1b
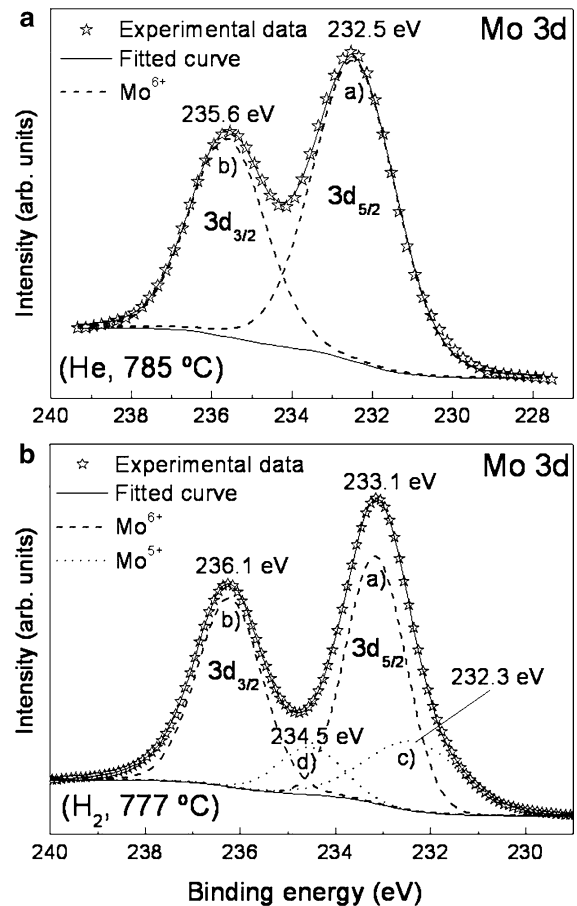

Fig. 1 Mo 3d spectra and curve fitting of samples grown under condition: a He, 785 °C and b H_2, 777 °C

was obtained by resolving the spectrum into four overlapping curves: (a), (b), (c), and (d). The binding energies of the higher intensity Mo 3d doublet were 233.1 eV (FWHM ~ 1.5 eV) and 236.1 eV (FWHM ~ 1.6 eV) corresponding to Mo^{6+}. The doublet of lower intensity was fitted with binding energies of 232.3 and 234.5 eV for the $3d_{5/2}$ and $3d_{3/2}$ levels, respectively. These binding energy values are close to reported values for Mo^{5+} (Sian and Reddy 2004).

Electron beam effects detected using TEM: irradiation damage

Figure 2 is a series of TEM images recorded at different irradiation times on a MoO_{3-x} rod-like structure grown under condition (H_2, 777 °C). The
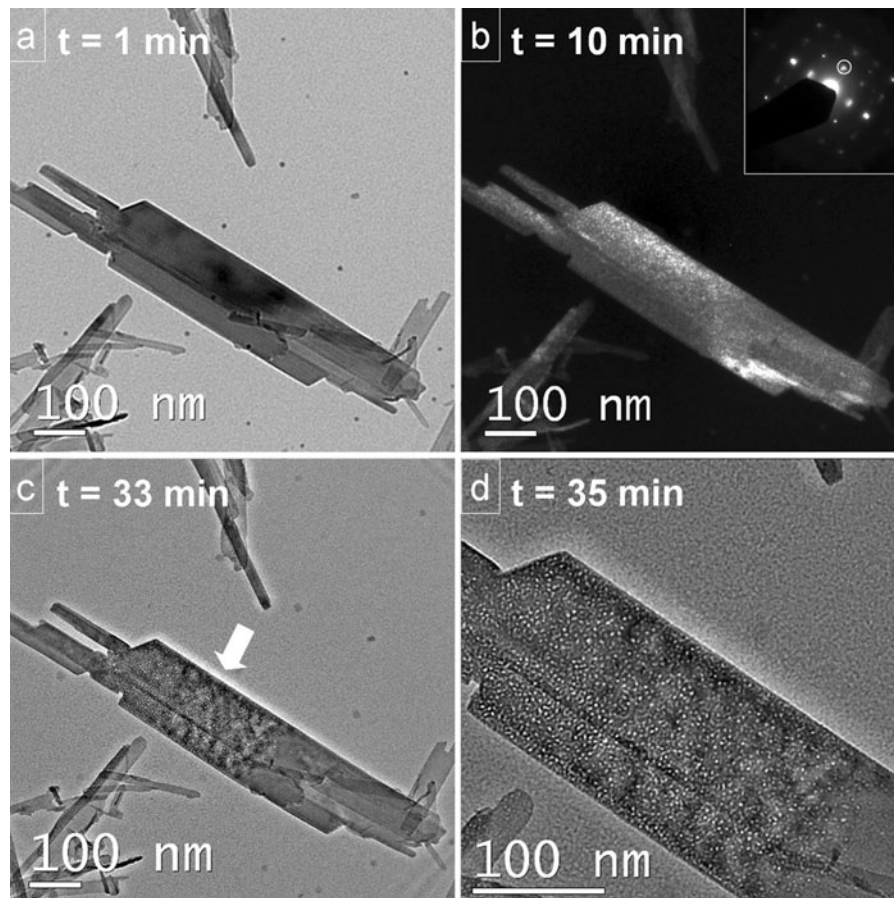
Fig. 2 TEM images showing the electron beam effects on a rod-like structure grown under condition (H$_2$, 777 °C). **a** Multi beam image recorded after 1 min of electron irradiation. **b** Dark field image recorded after 10 min (the *inset* is the SAED pattern). **c** Multi beam image recorded at 33 min showing the irradiation damage. **d** High magnification of **c** revealing the irradiated zone

electron beam was concentrated in an area of 100 nm in radius. Figure 2a was recorded after 1 min of electron irradiation. Figure 2b is a dark field image recorded after 10 min under electron beam irradiation and there are no detectable changes. The inset of Fig. 2b is the SAED pattern taken from the central region of the structure showing well-defined diffraction spots, revealing the single crystalline character of the structure. Figure 2c was taken after 33 min of irradiation showing an appreciable effect of the electron beam on the irradiated zone. Finally, Fig. 2d is a multi beam image recorded immediately after image 2c was taken, at 35 min of irradiation but with a higher magnification. This image reveals with better definition the damage caused by the electron beam, with an appearance similar to the one caused by a

spinodal decomposition. No changes were observed outside the irradiated zone.

Another example is shown in the bright field TEM images of Fig. 3. In this case, the sample was grown under condition (He, 664 °C) which resulted in MoO$_3$ nanostructures. Figure 3a is an image recorded at the beginning of the TEM examination (0.5 min) showing faceted particles as well as plates. Figure 3b, c is the high magnification images of the particle indicated by the arrow in Fig. 3a. Figure 3b was recorded after concentrating the electron beam for 1 min on the particle zone indicated by the framed circle in the figure. No changes are observed in this micrograph. However, Fig. 3c, recorded after 10 min of concentrated irradiation, shows that the time was sufficient to cause an evident damage of the particle, as revealed by
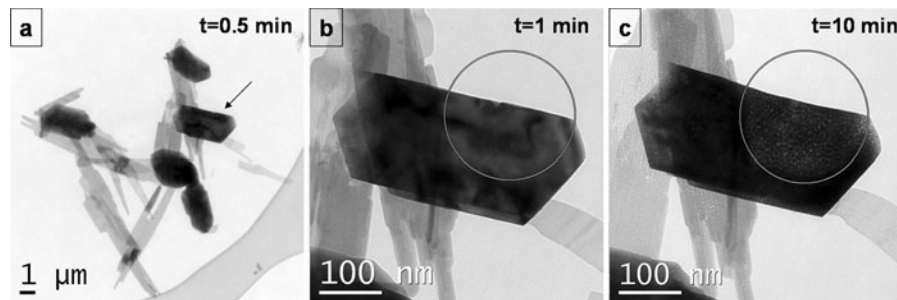
Fig. 3 TEM images revealing the electron irradiation-induced effects on a particle grown under condition (He, 664 °C). **a** Bright field TEM image recorded after 0.5 min of electron irradiation; **b**, **c** bright field images at high magnification of the particle indicated by the *arrow* in **a** after 1 and 10 min of electron irradiation, respectively

the changes in the image contrast of the affected zone as compared with the same zone shown in Fig. 3b.

Figure 4 shows a pair of bright/dark field TEM images of a MoO_{3-x} nanofiber grown under condition (H_2, 784 °C); both images were recorded after 5 min of concentrated incidence of the electron beam on a circular area of 80 nm in diameter. Figure 4a, b reveals the fiber of 23 nm of average width and the severe damage caused after only 5 min of exposure under the electron beam. The crystalline character of the nanostructure is indicated by SAED pattern shown in the inset of Fig. 4b which also shows the diffraction spot used for generating the dark field image. This decomposition phenomenon by a concentrated electron beam onto a localized area of the nanostructure is similar to that exhibited by the crystalline samples of Figs. 2 and 3, but in this case with a faster kinetics.

Structural transformations by irradiation: sequential changes of SAED patterns

Figure 5 depicts sequential changes of SAED patterns caused by the incidence of the electron beam concentrated on the framed area of the MoO_3 particle shown in Fig. 3b. The SAED pattern of Fig. 5a was recorded after 1.5 min of irradiation revealing the single crystalline character of the particle. The indexed diffraction spots can be attributed to the (110), (201), (041), and (002) planes of orthorhombic MoO_3 (α-MoO_3), consistent with the results provided by X-ray powder diffraction (not shown) for samples grown by condensation in helium. Figure 5b is a SAED pattern, recorded after 7 min of electron irradiation, exhibiting an evident change as compared with the pattern shown in Fig. 5a. The diffuse diffraction spots of the Fig. 5b indicate the formation of planar defects by aggregation
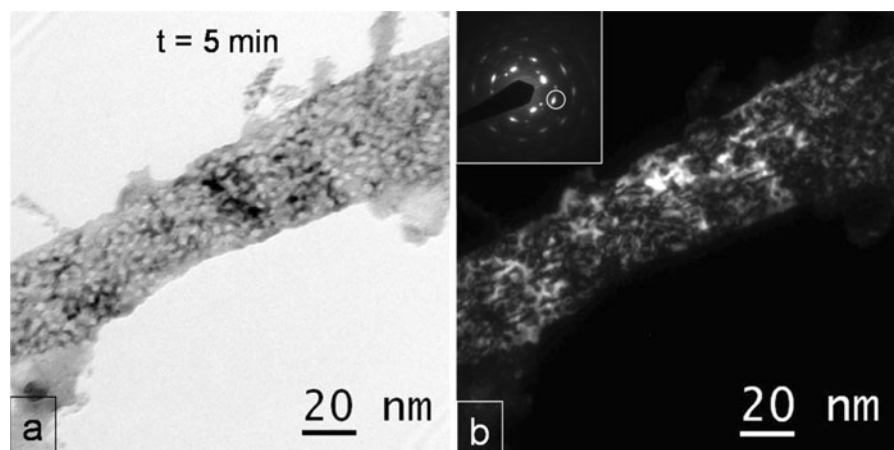

Fig. 4 Severe and fast damage caused by electron beam on a MoO_{3-x} nanofiber grown under condition (H_2, 784 °C). **a**, **b** Bright and dark field TEM images, respectively, recorded after 5 min of electron irradiation
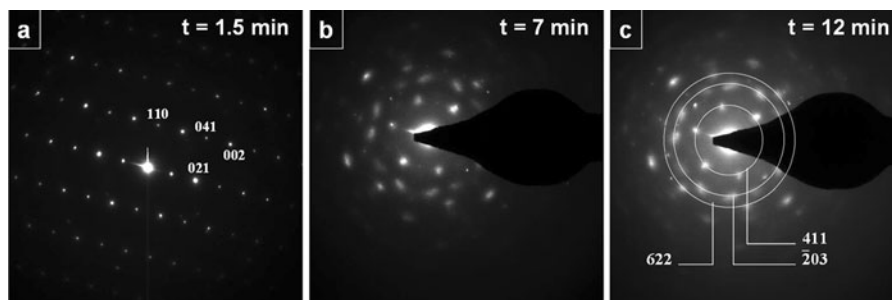
Fig. 5 **a**, **b**, **c** Sequential changes of SAED patterns recorded at different electron exposure times on the particle analyzed in Fig. 3

and accumulation of oxygen vacancies produced by the electron beam that reduce the oxide of the MoO_3 particle. The oxygen loss not only generates changes in the interatomic distances of the MoO_6 octahedra but also in their orientation (Wang et al. 2004). These structural changes would lead to degenerate the MoO_3 unit cell by local variation in all the original dimensions of the orthorhombic lattice parameters (Zuñiga 2008, personal communication). Figure 5c shows another SAED pattern recorded after 12 min of electron irradiation showing a pattern similar to the one shown in Fig. 5b but with slightly more intense diffuse diffraction spots. After 12 min of irradiation, no additional important structural changes take place with further irradiation. On the other hand, Fig. 5c shows three rings manually drawn on the pattern where different sets of spots are placed. The estimated interplanar distances from these rings do not match neither the starting orthorhombic MoO_3 nor MoO_2. A better fit can be obtained by assigning the rings to the (411), (−203), and (622) planes of monoclinic Mo_4O_{11} (γ-Mo_4O_{11}), which is a Magnéli's phase of molybdenum oxide (Vincent and Marezio 1989).

Another example of the electron beam-induced structural transformation of a crystalline nanostructure is shown in Fig. 6. These images were also acquired at different irradiation times by concentrating the electron beam on a MoO_3 nanoparticle of $\sim$40 nm in size grown under condition (He, 910 °C). Figure 6a, b is SAED patterns of the hexagonal nanoparticle whose morphology is revealed by the dark field image of Fig. 6c. Figure 6a is a diffraction pattern in the [1 −1 −2] zone axis recorded at the start of the TEM examination (0.5 min), showing the single crystalline character of the particle. This pattern is very similar to the one shown in Fig. 5a. The indexed diffraction spots can also be attributed to the (110), (201), (041), and (002) planes of α-MoO_3. Figure 6b shows a pattern recorded after 10 min of electron irradiation where the formation of diffraction rings is better defined. These discontinuous diffraction rings indicate the formation of crystals or grains not uniformly oriented in the new developed structure and, therefore, a structural evolution of the nanoparticle from a single crystalline character to a polycrystalline one. The indexed diffraction rings can be attributed to the (011),
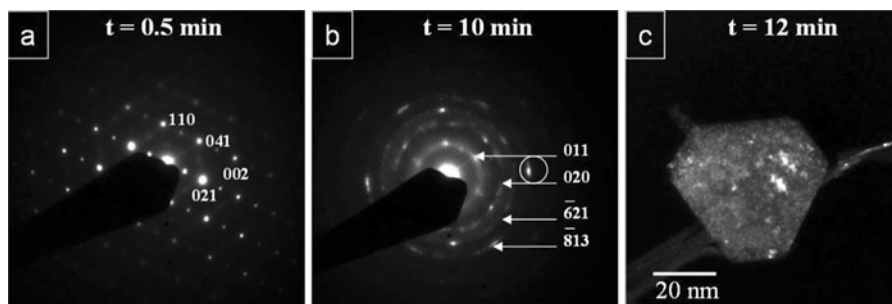

Fig. 6 Sequential changes at different irradiation times taken from a MoO_3 nanoparticle grown under condition (He, 910 °C). **a**, **b** SAED patterns from the particle shown in **c** and recorded after 0.5 and 10 min of electron irradiation, respectively. **c** Dark field TEM image of the irradiated particle after 12 min of irradiation

(020), (−621), and (−813) planes of γ-Mo_4O_{11}. Finally, Fig. 6c is a dark field TEM image showing the particle affected by the irradiation, this image was acquired immediately after recording the last pattern shown in Fig. 6b and it was generated using as illumination source the diffraction spot indicated by a circle in the pattern of Fig. 6b.

This final sequence of SAED patterns corroborated that the electron beam-induced structural transformation of the α-MoO_3 nanoparticles leads to a Magnéli's phase of the oxide whose kinetics basically depends on the local mass of the nanostructure that is irradiated.

Structure evolution revealed by dark field and HRTEM images

Figure 7 is a set of TEM images showing the structure evolution caused by the electron beam on a MoO_{3-x} nanorod grown under condition (H_2, 777 °C). Figure 7a is a bright field image that depicts a different zone of Fig. 2a, a nanorod of ~ 20 nm in width, i.e., smaller and lighter than the rod-like structure observed in Fig. 2. The framed part in Fig. 7a shows the zone of

the nanorod affected by the electron beam. Figure 7b, c is the dark field images recorded after 8 and 11 min, respectively, showing that the zones in diffraction condition change with irradiation time. The insets in Fig. 7b, c are SAED patterns showing in each case the diffraction spot used to generate the dark field image. Some diffraction spots disappear from the starting pattern due to the degeneration of the lattice planes and formation of CS planes in the molybdenum oxide structure (Rao and Raveau 1998). Figure 7d, e, and f is the HRTEM images revealing the effect of the CS planes formation. Figure 7d was recorded at the start of the TEM examination, after 1 min of electron irradiation. This image reveals well-defined lattice fringes. Figure 7e was recorded after 3.5 min of irradiation and shows the change in the image contrast arising by formation of CS planes and the high amount of defects that are quickly formed near the nanostructure surface. Finally, Fig. 7f was recorded after 13 min of electron irradiation showing a more pronounced change in the image contrast revealing that the irradiated zone is highly disordered: no starting lattice fringes are identified after this electron irradiation dose.
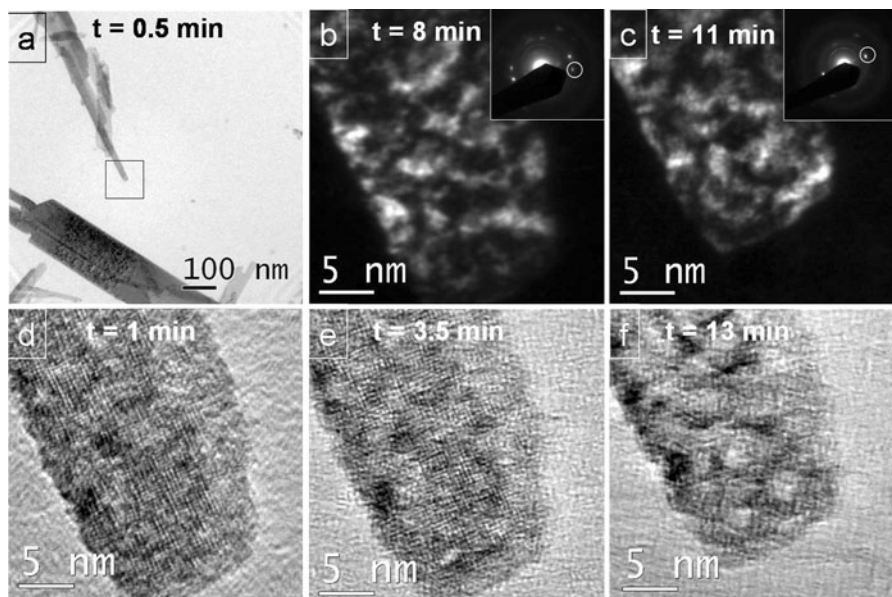

Fig. 7 Structure evolution of a MoO_{3-x} nanorod grown under condition (H_2, 777 °C). **a** Bright field TEM image showing the nanorod (the *frame* indicates the irradiated zone). **b, c** Dark field TEM images recorded after 8 and 11 min of electron exposure, respectively (the *insets* are SAED patterns). **d, e, f** HRTEM images recorded after 1, 3.5, and 13 min of irradiation, respectively
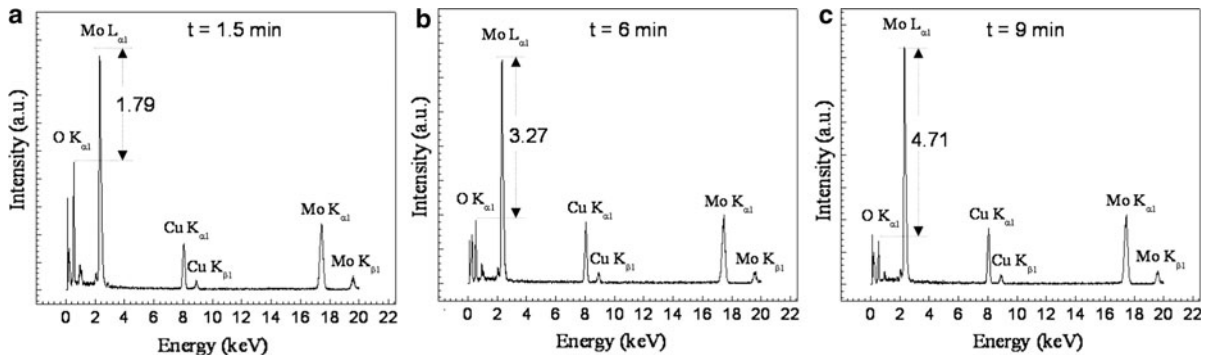
Fig. 8 EDS spectra of the nanorod shown in Fig. 7 recorded after **a** 1.5 min, **b** 6 min, and **c** 9 min of electron irradiation

Reduction process-induced structural changes: in situ EDS analysis

Figure 8 shows the EDS spectra of the nanorod shown in Fig. 7. Figure 8a is a spectrum recorded after 1.5 min of irradiation when no significant damage of the structure is still appreciated, as shown by the TEM image in Fig. 7d. The intensity ratio estimated between the peak value of Mo $L_{\alpha 1}$ and O $K_{\alpha 1}$ was 1.79 while this ratio increased to 3.27 after 6 min of electron irradiation, as shown in Fig. 8b. Finally, the spectrum of Fig. 8c acquired after 9 min of electron incidence shows that the intensity ratio was 4.71. This increase in the intensity ratios Mo $L_{\alpha 1}$/O $K_{\alpha 1}$ when the electron irradiation time increased indicates oxygen loss from the oxide nanostructure which promotes the CS planes mechanism in the first stage of oxide reduction and, finally, the development of a polycrystalline structure with oxygen-deficient grains.

Discussion

The electron beam effects of TEM involve specimen heating, electrostatic charging, knock-on displacement, radiolysis, sputtering, and hydrocarbon contamination (Egerton et al. 2004). Knock-on effect or radiolysis processes are considered to be the most common mechanisms responsible for the damage produced by electron radiation (Hobbs 1979; Hobbs and Pascucci 1980). The knock-on displacement is the elastic interaction between the incident electrons with atomic nuclei that causes the displacement of the atoms from their equilibrium sites and the creation of point defects as Frenkel defects (vacancy-interstitial

pair). The radiolysis process is the fastest interaction between the incident electrons and the atom electrons, which generates localized electronic excitations with sufficient energy that it can be converted to momentum of a departing atom or ion (Hobbs 1979).

In all the cases analyzed in this study, a long exposure to the electron beam in a large area of the nanostructure does not induce the same effect than the concentrated beam on a smaller area (25 or 100 nm in diameter). This suggests that the main mechanism responsible of the reduction process is not knock-on displacement but local heating. Knock-on is only related with the accelerating voltage of the electrons. On the contrary, electron beam heating is strongly dependent on the current density (A/cm^2) and the size of the irradiated sample. The thermal stimulus is more intense when the electron beam is concentrated onto smaller nanostructures, as the heat dissipation is expected to be lower than in crystalline structures of major size and mass, leading to a higher local temperature increase and, therefore, faster structural transformation kinetics. On the other hand, the growth conditions of these samples are very far from equilibrium and many of the nanostructures are believed to be metastable. Wang et al. (2004) reported a structural transformation in commercial powder of MoO_3 toward a reduced Mo-oxide after 40 min of irradiation using a high electron current density (57.6 A/cm^2). In our molybdenum oxide nanostructures, structure changes were produced in just 10 min of electron irradiation under the operating conditions of the TEM used in this study. However, the radiolysis effect is not ruled out in the irradiated oxide nanostructures as it would improve the diffusion rate (Zhang and Marks 1989) leading to a structural transformation in shorter

times, as presented here. It is still not clear if the transformation kinetics would be faster in MoO_{3-x} than in MoO_3 nanostructures. We believe that the heat dissipation would be lower in the MoO_{3-x} samples due to the oxygen vacancies present in the lattice, leading to a faster local heating and thus causing more intense irradiation damage in lower times.

Conclusions

The progressive incidence of an electron beam onto MoO_3 and MoO_{3-x} crystalline nanostructures generates damage and structural changes after a few minutes (3–10 min) of electron irradiation. As revealed by SAED patterns, a structural transformation from orthorhombic MoO_3 (α-MoO_3) to monoclinic Mo_4O_{11} (γ-Mo_4O_{11}) was observed. The structural changes are associated with oxygen loss from the oxide, as revealed by sequential EDS spectra recorded at progressive irradiation times. In the early stage of the reduction process, oxygen vacancies generated by the electron beam are accommodated by CS planes, as detected by HRTEM images. The mechanisms responsible in the oxide reduction by the electron beam can be attributed to the local heating of the irradiated area and to the radiolysis process.

References

Bertrand O, Dufour LC (1980) X-ray and electron microscopy investigation of the topotactic transformation of MoO_3 into MoO_2. Phys Stat Sol A60:507–519. doi:10.1002/pssa.2210600222

Bettahar MM, Costentin G, Savary L, Lavalley JC (1996) On the partial oxidation of propane and propylene on mixed metal oxide catalysts. Appl Catal A 145:1–48. doi:10.1016/0926-860X(96)00138-X

Bursill LA (1969) Crystallographic shear in molybdenum trioxide. Proc R Soc Lond A 311:267–290. doi:10.1098/rspa.1969.0118

Delannay F (1982) On the reduction of orthorhombic MoO_3 to MoO_2. Phys Stat Sol A 73:529–537. doi:10.1002/pssa.2210730228

Diaz-Droguett DE, Fuenzalida VM (2010) One-step synthesis of MoO_3 and MoO_{3-x} nanostructures by condensation in gas: effect of the carrier gas. J Nanosci Nanotechnol 10:6694–6706. doi:10.1166/jnn.2010.2520

Diaz-Droguett DE, Fuenzalida VM, Diaz-Espinoza MS, Solórzano G (2008a) Electron beam effects on amorphous molybdenum oxide nanostructures grown by condensation in hydrogen. J Mater Sci 43:591–596. doi:10.1007/s10853-007-1602-1

Diaz-Droguett DE, Fuenzalida VM, Solórzano G (2008b) Nanostructures of crystalline molybdenum trioxide grown by condensation in a carrier gas. J Nanosci Nanotechnol 8:5977–5984. doi:10.1166/jnn.2008.332

Egerton RF, Li P, Malac M (2004) Radiation damage in the TEM and SEM. Micron 35:399–409. doi:10.1016/j.micron.2004.02.003

Fleisch TH, Zajact GW, Schreiner JO, Mains GJ (1986) An XPS study of the UV photoreduction of transition and noble metal oxides. Appl Surf Sci 26:488–497. doi:10.1016/0169-4332(86)90120-0

Grasselli RK (1999) Advances and future trends in selective oxidation and ammoxidation catalysis. Catal Today 49:141–153. doi:10.1016/S0920-5861(98)00418-0

Haber J, Lalik E (1997) Catalytic properties of MoO_3 revisited. Catal Today 33:119-137. doi:10.1016/S0920-5861(96)00107-1

Henrich VE, Cox PA (1994) The surface science of metal oxides. Cambridge University Press, Cambridge

Hobbs LW (1979) Introduction to analytic electron microscopy. Plenum Press, New York

Hobbs LW, Pascucci MR (1980) Radiolysis and defect structure in electron-irradiated α-quartz. J Phys Colloq 41:C6-237–C6-242. doi:10.1051/jphyscol:1980660

Magnéli A (1953) Structures of the ReO_3-type with recurrent dislocations of atoms: 'homologous series' of molybdenum and tungsten oxides. Acta Cryst 6:495–500. doi:10.1107/S0365110X53001381

Rao CNR, Raveau B (1998) Transition metal oxides: structure, properties, and synthesis of ceramic oxides. Wiley-VCH, New York

Sian TS, Reddy GB (2004) Optical, structural and photoelectron spectroscopic studies on amorphous and crystalline molybdenum oxide thin films. Sol Energy Mater Sol Cells 82:375–386. doi:10.1016/j.solmat.2003.12.007

Su DS (2002) Electron beam induced changes in transition metal oxides. Anal Bioanal Chem 374:732–735. doi:10.1007/s00216-002-1377-9

Vincent H, Marezio M (1989) Low dimensional electronic properties of molybdenum bronzes and oxides. Kluwer Academic Publishers, Dordrecht

Wagner CD, Riggs WM, Davis LE, Moulder JF, Muilenberg GE (1979) Handbook of X-ray photoelectron spectroscopy, Physical Electronics Division, Perkin-Elmer, Eden Prairie, MN

Wang D, Su DS, Schlögl R (2004) Electron beam induced transformations of MoO_3 to MoO_2 and a new phase MoO. Z Anorg Allg Chem 630:1007–1017. doi:10.1002/zaac.200400052

Zhang JP, Marks LD (1989) Symmetry in DIET phase transitions. Surf Sci 222:13–20. doi:10.1016/0039-6028(89)90330-0